On the efficiency of spatial channel reuse in ultra-dense THz networks

V. Petrov, D. Moltchanov, Y. Koucheryavy
Nano Communications Center
Department of Electronics and Communications Engineering
Tampere University of Technology, Tampere, Finland
Email: vitaly.petrov@tut.fi, dmitri.moltchanov@tut.fi, yk@cs.tut.fi

***Abstract*—Wireless communications in the terahertz (THz) frequency band, 0.1–10THz, promise a rapid increase of channel capacity in next-generation networks. However, the advantages of this technology depend not only on the single link performance, but also on the possibility of several THz links to coexist in the same area. Thus, the efficiency of spatial channel reuse has to be studied. Due to the presence of specific effects in the THz band, such as molecular absorption and molecular noise, existing performance evaluation techniques are not straightforwardly applicable. In this paper, the approach for network-level analysis of THz wireless communications is proposed. This approach is based on the tools of stochastic geometry and takes into account the specific signal propagation features of the THz frequency band. The presented technique is used to derive the distribution of SINR and spectral efficiency as well as to estimate the optimal distance between receiving nodes and maximize the area capacity.**

I. Introduction

Tactile Internet (TI), as a deep evolution of 5G, is the novel technology trend characterized by extremely low latency in combination with high availability, reliability and security [1]. To fulfill the proposed set of requirements numerous communication and networking technologies has to be properly adjusted, upgraded, or even completely redesigned. These include medium access and multiple access control techniques, forwarding and routing of messages through the network, cloud-based and distributed application servers, existing interfaces for user interaction and many others.

One of the concepts to be reconsidered following the TI paradigm is the Internet of Nano Things (IoNT), based on modern networks of micro- and nano-scale sensor devices. Originally suggested to be built on top of delay-tolerant communication technologies with major focus on maximizing the energy-efficiency and uptime value, the IoNT systems have to take into account one more criterion – minimizing the message propagation time. This criterion is motivated by the TI requirement for maximum end-to-end delay between the user request and the system response, currently set to 1ms [1].

With respect to such a strict requirement, the use of THz frequency band, 0.1–10THz, for IoNT, suggested in [2], seams appropriate. Such high frequencies promise extremely high capacity at the air interface in the range of few terabits per second [3] and, at the same time, potentially allow for very small antennas of few tens of micrometers in size [4]. These properties would enable development of small transceivers communicating at extremely high bit rates giving rise to future IoNT solutions.

IoNT systems are expected to be characterized by highly dense deployments. In this environment the message propagation through the network following the conventional ad-hoc approach – send all the collected information to neighbors – becomes very slow and energy inefficient due to substantial number of devices being involved in communication. The feasibility of alternative approach, where nodes report to the most distant node aiming to minimize the number of hops, is also questionable for dense deployments due to the need for complicated multiple access and routing as the interference level can easily forbid communications over some of the links.

To deal with the abovementioned issue, we introduce a two-tier network topology with dedicated receiving devices deployed with intensity of several orders lower than primary sensor nodes. These receivers can be deployed either permanently in conjunction with the sensors or on-demand, e.g. on a portable scanning device. The role of these stations is to collect, process and report the aggregated data to the user or the remote application server. The major question for the proposed topology is how dense should the receivers be deployed to minimize the reporting time. In other words, we are interested in the most efficient spatial channel reuse. To find this optimal point, the effect of interference between coexisting links in THz networks has to be studied.

In this paper, we develop an analytical model for the ultra-dense THz network capable of capturing the mean values and distributions of Signal-to-Noise-plus-Interference-Ratio (SINR), spectral efficiency and area capacity. Due to the presence of non-linear effects in THz signal propagation through the medium, such as molecular absorption and molecular noise, we cannot apply the closed-form solutions derived originally for multi-cell cellular networks. Instead, using the primitives from stochastic geometry, we derive the expressions for the metrics of interest specifically for the THz band. We apply our model to study the interference between neighboring links, evaluate the proposed two-tier network topology and, finally, find the optimal distance between the receiving nodes. The presented analysis provides an important step towards the network-level evaluation of THz wireless communications.

The rest of the paper is organized as follows. In Section II, we summarize the previous work done in the field of study by

978-1-4799-5952-5/15/$31.00 ©2015 IEEE

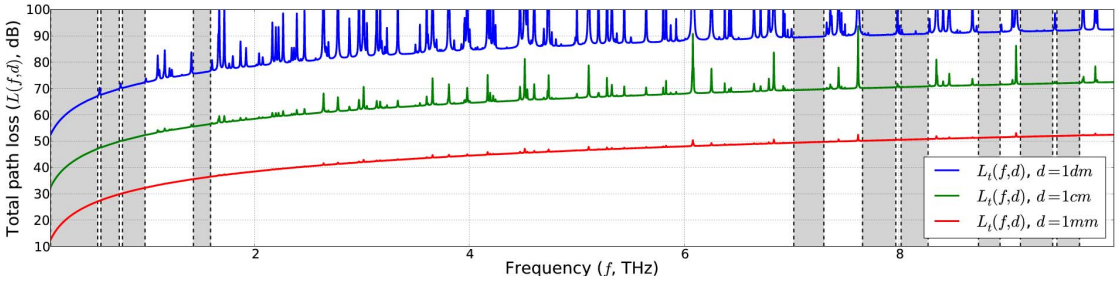

Fig. 1. The total path loss, $L_t(f,d)$, and transparency windows in the THz frequency band.

reminding the point-to-point signal propagation model in THz networks and existing approaches for network-level analysis of wireless communication technologies. We then specify the scenario of interest defining the related area capacity optimization problem in Section III. In Section IV, we present our analytical approach for network performance evaluation. Finally, we demonstrate and analyze our results in Section V. Conclusions are drawn in the last section.

II. Related Work

A. THz Propagation and Noise Models

The THz band, 0.1–10THz, is characterized by a number of unique propagation features. Following [5], the propagation loss in point-to-point line-of-sight (LOS) communication scenario depends on both frequency of operation f and separation distance d as

$$L(f,d) = \frac{1}{L_A(f,d)L_P(f,d)}, \tag{1}$$

where $L_A(f,d)$ is the absorption loss due to water vapor and $L_P(f,d)$ is the free-space propagation loss given by

$$L_P(f,d) = \left(\frac{4\pi f d}{c}\right)^2, \tag{2}$$

where c is the speed of light.

The absorption loss is a feature distinguishing 0.1–10THz band from radio frequencies. Following [6], it is inverse proportional to the transmittance of the medium, $\tau(f,d)$, as

$$L_A(f,d) = \frac{1}{\tau(f,d)}, \tag{3}$$

where $\tau(f,d)$ obey Beer-Lambert law, $\tau(f,d) = e^{-K(f)d}$, and $K(f)$ is the absorption coefficient available from [7].

Thus, the received signal psd can be estimated as

$$P_R(f,d) = \frac{P_T}{L(f,d)} = P_T(f)\frac{c^2}{16\pi^2 f^2} d^{-2} e^{-K(f)d}. \tag{4}$$

Fig. 1 demonstrates the total path loss in the THz band, $L(f,d)$. As one can observe, the THz wireless channel is highly frequency-selective with several so-called *transparency windows* – sub-bands, where absorption loss, $L_A(f,d)$, tends to zero. These transparency windows are frequency bands most suitable for communications.

The noise in THz band comes from two sources: (i) thermal agitation of electrons in semiconductors and (ii) molecular absorption. The first part, also known as Johnson-Nyquist or thermal noise, is frequency dependent for THz band. Over the frequencies of interest it could be approximated by [8]

$$P_{TN}(f) = \frac{hf}{\exp(hf/k_B T) - 1}, \tag{5}$$

where h stands for the Planck's constant.

The molecular noise is caused by re-emission of a part of absorbed energy by molecules back to the environment. Following [9], [6], molecular noise psd is given by

$$P_{MN}(f,d) = \frac{S_{Tx}(f)}{L_P(f,d)}[1 - \tau(f,d)]. \tag{6}$$

The total noise psd is obtained as the sum of (5) and (6).

B. System-Level Analysis

The question of efficient spatial frequency reuse has been addressed for numerous systems including sensor networks [10], general ad-hoc environment [11] and, recently, in context of device-to-device communications [12]. Most studies rely on the use of Poisson Point Process (PPP) as it has been found to provide first-order approximation of nodes positions [13]. Applying the methods of stochastic geometry one could characterize basic performance metrics of these systems including Signal-to-Interference-plus-Noise Ratio (SINR), Shannon capacity and throughput obtained by a station of interest [14].

In most analytical studies the received signal power has been assumed to follow $P_R(d) = Ad^{-\gamma}$, where d is the separation distance between transmitter and receiver, while A and γ are propagation dependent constants. This model leads to a simple expressions of the received signal strength and aggregated interference as a function of the random distances to the transmitter of interest, d_0, and interferers, d_i, $i = 1, 2, \ldots, N$. Furthermore, as the only source of noise below THz is thermal noise, which is flat up until approximately 0.1THz, the expression for SINR is the ratio of two independent random variables. Thus, it is feasible to get a closed-form expression for SINR and its derivatives in a Poisson field of interference.

In THz band the expression for SINR has a significantly more complex structure involving dependent random variables due to the presence of molecular noise. On top of this, the received signal strength in the form of $P_R(d) = Ad^{-\gamma}e^{-K(f)d}$ posses additional challenges that may prevent closed-form expressions for the metrics of interest.

III. Scenario Definition

A. Deployment

In this paper, we consider a highly dense network environment. Assume that there is a certain entity deciding on

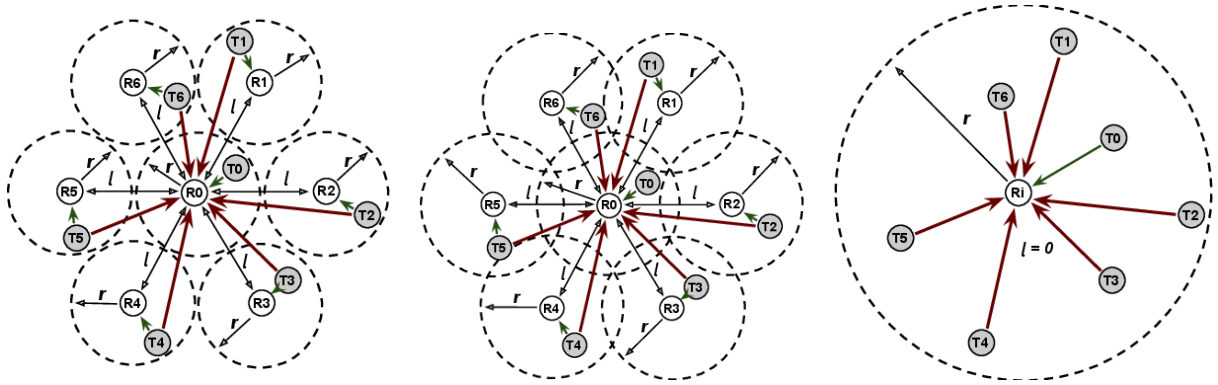

(a) Separation $l = 2r$ (b) Separation $0 < l < 2r$ (c) Separation $l = 0$

Fig. 2. CPU architectures.

link establishment in the network. The scheduling of links happens at discrete instants of time, that is, the network controller decides which links must be on during the next time interval Δ. To deal with the interference, the network controller implements the following interference protection. If a certain node is designated as a receiver at time t then the intended transmitter is located anywhere within the radius r while no other transmitters acting on R_0 as interferers are located closer than at r. In this case, the distance between any two adjacent receivers is exactly $l = 2r$. Starting with this case and concentrating on the arbitrarily chosen receiver (tagged receiver) we identify the following three scenarios.

The case resulting in best possible (on average) SINR is shown in Fig. 2(a). However, the area covered in this case, is the biggest out of all those we consider. Even though we should get the best capacity, the area capacity might not be maximized. Let us now shorten the distance between two receivers by getting them closer to each other while preserving the distance between adjacent receivers as illustrated in Fig. 2(b). In this case, the interferers could be closer to the tagged receiver resulting in lower SINR compared to the previous case. However, at the same time, the area covered is getting smaller and it may potentially drive the area capacity higher. Decreasing the distance between adjacent receivers further we eventually end up with all the receivers co-located at the same point as shown in Fig. 2(c). Most likely this configuration will result in the worst possible SINR but, at the same time, in the smallest possible covered area. While decreasing the distance between adjacent receivers from $2r$ to 0 there might be an optimal point allowing to maximize the use of resources in THz networks. We will identify this point next.

B. Metrics of Interest

The first metric we take into account is SINR, defined as

$$S(\vec{d}, \vec{P}_T, f) = \frac{P_{R_0}(d_0, P_T, f)}{I(\vec{P}_T, \vec{d}, f) + N(\vec{P}_T, \vec{d}, f)}, \tag{7}$$

where $P_{R_0}(d_0, P_T, f)$ is the received signal psd at the distance d_0, $I(\vec{P}_T, \vec{d}, f)$ is the aggregate psd of the interferers at the receiver, $N(\vec{P}_T, \vec{d}, f)$ is the noise psd at the receiver, $\vec{d}$ is the vector of separation distances, d_i, $i = 1, 2, \ldots, 6$, between interferers and the receiver, f is the operating frequency and M is the number of interfering nodes. In this study, we assume no power control and assign $P_{T_i} = P_{T_j}$, $i, j = 0, 1, \ldots, N$. For simplicity of notation, in what follows, for SINR, interference and noise functions we drop arguments that are often silently assumed, f, P_T and d_i.

The received useful power is given by

$$P_R = Ad_0^{-2}e^{-Kd_0},\ A = \frac{P_T c^2}{16\pi^2 f^2}. \tag{8}$$

The aggregate interference from six transmitters is then

$$I = A\sum_{i=1}^{6} d_i^{-2}e^{-Kd_i}. \tag{9}$$

The noise power is written as

$$N = N_0 + A\sum_{i=0}^{6} d_i^{-2}(1 - e^{-Kd_i}), \tag{10}$$

where $N_0 = k_B T$ and we take into account molecular noise caused by T_0 as the sum starts with $i = 0$. Since

$$Ad_i^{-2}(1 - e^{-Kd_i}) + Ad_i^{-2}e^{-Kd_i} = Ad_i^{-2}, \tag{11}$$

the denominator of (7) can be written as

$$I + N = N_0 + Ad_0^{-2}(1 - e^{-Kd_0}) + A\sum_{i=1}^{6} d_i^{-2}. \tag{12}$$

Substituting (8) and (12) into (7) gives

$$S = \frac{Ad_0^{-2}e^{-Kd}}{N_0 + Ad_0^{-2}(1 - e^{-Kd_0}) + A\sum_{i=1}^{6} d_i^{-2}}. \tag{13}$$

When there is no thermal noise, A in numerator and denominator of (13) cancels out making SINR independent of the emitted power while derivations below simplify. In what follows, we address the general case of non-zero thermal noise.

In addition to SINR, we also focus on spectral efficiency,

$$E = E(\vec{d}, \vec{P}_T, f) = \log_2[1 + S(\vec{d}, \vec{P}_T, f)], \tag{14}$$

area spectral efficiency, $E_A = E/V$, and area capacity, $C_A = BE/V$, where V is the area covered by communicating stations, and B is the used bandwidth.

IV. Network Analysis

A. Methodology Overview

Using (13) to evaluate SINR is rather complicated. However, the given scenario posses a number of interesting properties and allows for few simplifications making it feasible.

In the numerator and denominator of (13) the interference and the received signal terms are independent from each other. However, the molecular noise term, $Ad_0^{-2}(1-e^{-Kd_0})$, depends on the received power due to sharing the same distance d_0. To alleviate this issue, we propose to approximate the dependence between these two random variables using the correlation coefficient between them. That is, we replace $Ad_0^{-2}(1-e^{-Kd_0})$ by $kAd_0^{-2}e^{-Kd_0}$, where k is the correlation coefficient between two random variables, making SINR approximation possible.

Another important observation is that the distances from any interferer to the tagged receiver are independent and identically distributed (iid) for any $l \geq 0$. This allows to apply the central limit theorem when estimating the aggregate interference.

The scenario is addressed using three different cases: (i) $l = 0$, (ii) $r < l < 2r$, and (iii) $0 < l < r$. The reason to consider the latter case separately is that the distribution of the distance to a point randomly distributed within a circle from a fixed point located inside the circle is not readily available.

B. Interference Estimation

For all introduced cases, we apply the same methodology for interference modeling. First, we determine moments of the interference from a single node and then apply the central limit theorem to approximate the aggregated interference.

1) Case $l = 0$: Recalling Fig. 2(c), we see that all the receivers are co-located at the same point. Assuming that interferers are uniformly distributed in the circle of radius r, the probability density function (pdf) of the distance to R_0 is

$$f_D(d) = 2d/r^2,\ 0 < d < r. \tag{15}$$

Define a new random variable $G = 1/D^2$ expressing the interference from a single node. We see that due to iid nature of D_i these random variables are also iid. However, these random variables do not have moments as the integrals

$$E[G^v] = \int_0^R \frac{2x}{R^2}\left(\frac{1}{x^2}\right)^v dx \tag{16}$$

do not converge (the integrand is infinite as it gets to 0).

To deal with this issue, the following approximation is applied. We assume that the transmitters cannot be located closer than a certain very small distance $r_\star$ from the receiver. This assumption is warranted from the practical point of view, especially, taking into account that $r_\star$ can be chosen as small as needed and $r_\star \ll r$. In this case, the distance to R_0 is

$$f_D(d) = 2d/(r^2 - r_\star^2),\ r_\star < d < r, \tag{17}$$

and $G = 1/D^2$ has finite mean and variance

$$E[G] = (\ln r - \ln r_\star)/(r^2 - r_\star^2),$$
$$\sigma^2[G] = \frac{1}{2r_\star^2 r^2} - \left(\frac{\ln r - \ln r_\star}{r^2 - r_\star^2}\right)^2. \tag{18}$$

The parameters of Normal approximation are then given by

$$\mu = 6E[G],\ \sigma^2 = 36\sigma^2[G]. \tag{19}$$

2) Case $r < l < 2r$: The pdf of the distance to R_0 is [15]

$$f_D(d) = 2d\phi/\pi r^2,\ r < d < 3r, \tag{20}$$

where $r_1 = l - r$ and

$$\phi = \cos^{-1}\left(\frac{r_1}{d} + \frac{d^2 - r_1^2}{2d(r + r_1)}\right). \tag{21}$$

The moments of $G = 1/D^2$ are computed numerically using

$$E[G^v] = \int_{l-r}^{2r-l} \frac{2x\phi}{\pi r^2}\left(\frac{1}{x^2}\right)^v dx. \tag{22}$$

The moments of aggregate interference are found as in (19).

3) Case $0 < l < r$: In this case, the pdf of the distance to R_0 cannot be obtained using geometrical arguments as in [15] due to special behavior of $\cos^{-1}$ for $0 < l < r$. Indeed, the argument of the inverse cosine evaluates to values outside the domain of $\cos^{-1}(x) = \arccos(x)$ and the resulting density is complex. However, the real part still correctly describes the distance of interest. That is, for $0 < l < r$ we have

$$f_D(d) = \Re(2d\phi/\pi r^2),\ 0 < d < 2r, \tag{23}$$

where $\Re$ denotes the operation of taking the real part.

The general algebraic approach for finding distribution of the distance from a fixed point to a point uniformly distributed in a circle is sketched in Appendix. The moments of aggregate interference are found similarly to (19).

C. Distributions of Metrics of Interest

Once the distribution of aggregate interference is approximated, we can proceed with SINR derivation treating the abovementioned three cases similarly. However, finding SINR pdf directly is impossible as there is no analytic inverse of

$$f(x, y) = \frac{Ae^{-Kx}x^{-2}}{A(1 - e^{-Kx})x^{-2} + y}, \tag{24}$$

and the noise term depends on the received power. Therefore, we first find the numerator of SINR and then proceed with SINR pdf. The latter is accomplished by approximating the dependence between $Ae^{-Kx}x^{-2}$ and $A(1 - e^{-Kx})x^{-2}$ using the coefficient of correlation.

1) Numerator of SINR: The numerator of (13) is a function of a single random variable. Its density can be found as a special case of the method explained in Appendix. Recall that pdf of a random variable Y, $w(y)$, expressed as a function $y = \phi(x)$ of another random variable X with pdf $f(x)$ is [16]

$$w(y) = \sum_{\forall i} f(\psi(y))|\psi'(y)|, \tag{25}$$

where $x = \psi(y) = \phi^{-1}(x)$ is the inverse function.

The inverse of $y = \phi(x) = Ae^{-Kx}x^{-2}$ has two branches

$$x_{1,i} = \psi(y) = \frac{2}{K}W\left(\pm\frac{AK^2\sqrt{y/aK^2}}{2y}\right), \tag{26}$$

where $W(\cdot)$ is the Lambert W function [17].

The derivatives are given by

$$\psi'(y) = \frac{-W\left(\pm[2\sqrt{y/AK^2}]^{-1}\right) - 1}{Ky(W(\pm[2\sqrt{y/AK^2}]^{-1}) + z1)}. \quad (27)$$

Substituting (26) and modulo of (27) into (25) we get the distribution of the numerator of (13). Note that due to the presence of the Lambert W function, there is no closed form for this density. However, it can be numerically computed for any value of interest.

2) SINR distribution: Once the distribution of a random variable $X = Ae^{-Kd_0}d_0^{-2}$ is obtained, SINR could be written as $S = X/(Y + Z)$. To derive the density of S, we cannot proceed with methodology outlined in Appendix. The reason is that we are not able to define the joint pdf $f_{XYZ}(x, y, z)$, due to a dependence between X and Y via a common distance d_0. To obtain the accurate approximation, we suggest to evaluate the dependence between these random variables by expressing Y as a function of X in the form $Y = kX$, where k is the normalized correlation coefficient between Y and X,

$$k = (E[XY] - E[X]E[Y])/\sigma[X]\sigma[Y], \quad (28)$$

where $\sigma[X]$ and $\sigma[Y]$ can be found as

$$\sigma[X] = \sqrt{E[X^2] - (E[X])^2}. \quad (29)$$

The covariance between X and Y is then given by

$$Cov(X, Y) = E[Ae^{-Kd}d^{-2}A(1 - e^{-Kd})d^{-2}] = \\ = A^2(E[d^{-4}e^{-Kd}] + E[d^{-4}]). \quad (30)$$

Disallowing the transmitter T_0 to be infinitesimally close to the tagged receiver R_0 and recalling that the pdf of distance between them is $f_d(D) = 2d/(r^2 - r_\star^2)$, see (17), we have

$$E[d^{-4}] = \int_{r_\star}^{r} \frac{2x}{r^2 - r_\star^2}\frac{1}{x^4}dx = \frac{1}{r^2 r_\star^2}, \quad (31)$$

Denoting $B = 2/(r^2 - r_\star^2)$,

$$E[e^{-Kd}d^{-4}] = B\int_{r_\star}^{r} \frac{x}{e^{Kd}x^4}dx = \\ = B\left(\frac{K^2x^2Ei(-Kx) + Kxe^{-Kx} - e^{-Kx}}{2x^2}\bigg|_{r_\star}^{r}\right), \quad (32)$$

where $Ei(x) = -\int_x^\infty (e^{-y}/y)dy$ is an exponential integral.

First and second moments needed to find (28) and (29) are

$$E[X] = B\left(Ei[-Kx]\Big|_{r_\star}^{r}\right),$$
$$E[Y] = B\left(\ln x\Big|_{r_\star}^{r} - E[X]\right),$$
$$E[X^2] = B\left(\frac{4K^2x^2Ei(-2Kx) + 2Kxe^{-2Kx} - e^{-2Kx}}{2x^2}\bigg|_{r_\star}^{r}\right),$$
$$E[Y^2] = B\left(\left[-\frac{1}{2x^2}\right]\Big|_{r_\star}^{r} - E[X^2]\right). \quad (33)$$

Now, SINR can be approximated as

$$S = X/(kX - Y). \quad (34)$$

We get density of (34) according to the approach outlined in Appendix with some minor modifications owning to simplicity of the function. The joint pdf of X and Y is given by a direct multiplication of densities of Normal distribution with parameters μ and σ found in Section IV-B and that of $X = Ae^{-Kd_0}d_0^{-2}$ found previously in this section. Derivatives of $g(x, y) = x/(kx + y)$ with respect to x and y are

$$\frac{\partial g(x,y)}{\partial x} = \frac{y}{(kx+y)^2}, \frac{\partial g(x,y)}{\partial y} = -\frac{x}{(kx+y)^2}, \quad (35)$$

leading to the following Jacobian (see Appendix)

$$J = \begin{vmatrix} 1 & 1 \\ \frac{y}{(kx+y)^2} & \frac{-x}{(kx+y)^2} \end{vmatrix} = -\frac{x+y}{(kx+y)^2}. \quad (36)$$

Finally, the forward and inverse functions are

$$\begin{cases} u = kx + y \\ v = \frac{x}{kx+y} \end{cases}, \begin{cases} x = uv \\ y = u(1 - kv) \end{cases}. \quad (37)$$

Combining (36) and (37) we fist obtain joint pdf $f_{UV}(u, v)$ and then integrate out to find the pdf of SINR. Similarly, we could get densities of $10\log_{10} S$, spectral efficiency, area spectral efficiency, and area capacity. Note that the resulting densities cannot be expressed in elementary functions. Due to this and the lack of space their final forms are not presented. However, they still can be calculated as accurately as one needs as involved non-elementary functions, inlcuding exponential integral, $Ei(x)$, and Lambert W function, $W(x)$, can be computed with any given accuracy.

V. Numerical Results

In this section, we validate the proposed framework comparing our results with the ones produced by our modeling tool that simulates the deployment scenario. We then solve the optimization problem finding the distance l maximizing the network capacity. The considered medium is air with 1.6% of water vapor, $T = 300$K, and pressure of 10^5Pa. Transmit power of a node is set to 1μW.

We start with demonstrating the pdf of SINR obtained in (34-37) and numerical integration according to (43) for different values of r and l. As shown in Fig. 3(a), the analytical results closely resemble those obtained in simulations. For the range of l and r the form of the distribution does not remind any known continuous distribution implying that no simple approximations would suffice. The average value of SINR highly depends on the inter-receiver distance, l. For instance, for l value one order of magnitude higher than r the influence from the neighboring links is negligible. However, if l and r are the same, the level of interference at the receiver is comparable to the level of the received signal power resulting in SINR being around 5dB. Finally, when the interfering links are placed very close to each other ($l = 1mm$ in Fig. 3(a)) the effective simultaneous communications are hardly possible due to the SINR value being much lower 0. Although there

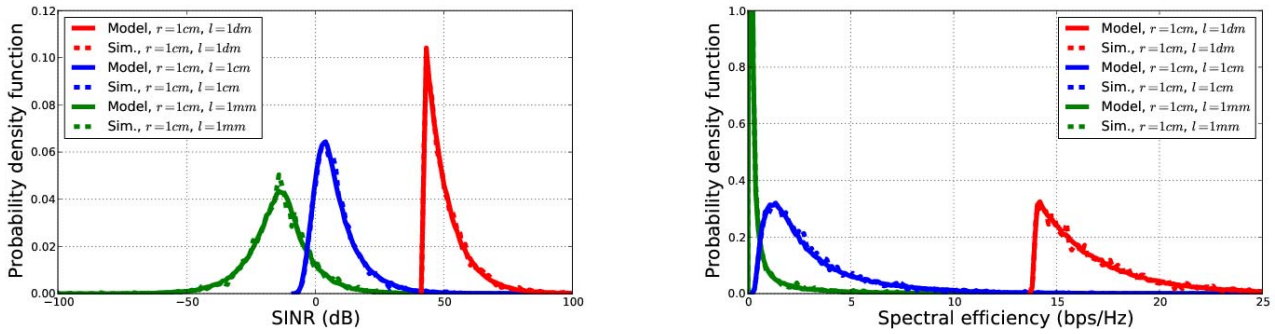

(a) SINR (b) Spectral efficiency

Fig. 3. Probability density functions of SINR and spectral efficiency.

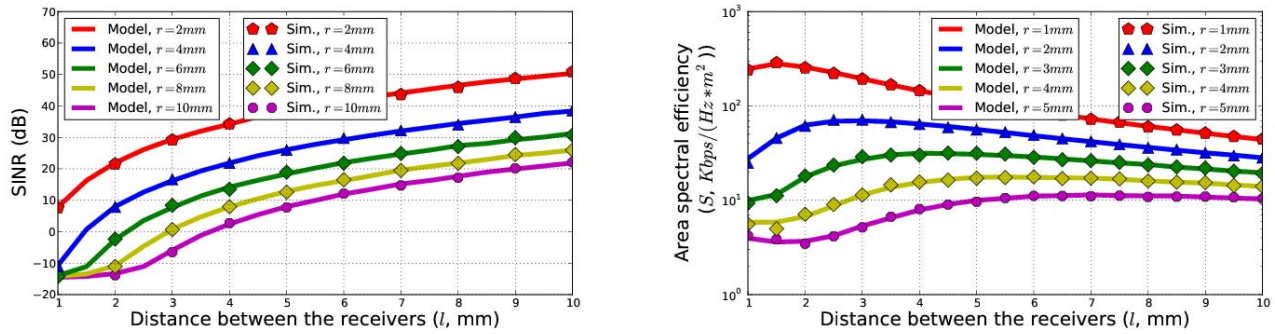

(a) SINR (b) Area spectral efficiency

Fig. 4. Effect of spatial reuse on network performance.

are modulations allowing to tolerate extremely low values of SINR (e.g. CDMA), it is highly unlikely that they can be used for power- and complexity-constrained THz micro- and nano-scale transceivers.

To study the effect of SINR degradation, Fig.4(a) shows the average SINR versus the distance between the receivers, l, for a number of values of r. The analytical results are obtained by numerical integration of the SINR densities. As one may observe, SINR passes the 0dB point, when l is at least $0.7r$. This is the minimum distance between receivers to enable simultaneous links in THz frequency band. However, having positive SINR only is not sufficient to claim the links are chosen properly. Therefore, we also have to investigate the behavior of spectral efficiency in dense THz networks.

Fig. 3(b) demonstrates densities of spectral efficiency for 1THz frequency and the same distances, as in Fig. 3(a). The analytical results are derived as $\log_2(1+S)$, similarly to SINR. The value of spectral efficiency for $l = 1$mm is around 0, while for inter-receiver distance of 1cm and 1dm the average value is around 2 and 13bps/Hz, respectively. These results correspond to what we observe in Fig. 3(a) and confirms our conclusion regarding the minimum tolerable distance between the receiving nodes to enable simultaneous communications.

Observe that the presented results suggest that the best performance is achieved when the network is as disperse as possible. In particular, both average SINR and spectral efficiency are maximized, when the distance between the receivers tends to infinity. However, this does not imply the deployment is optimal. To deal with this issue and investigate the spatial channel reuse in dense scenario, we focus on area-dependent metrics, area spectral efficiency and area capacity.

The average area spectral efficiency, expressed in Kbps/Hz·m^2 is shown in Fig. 4(b) for different values of l and r. As one observes, the metric of interest has a maximum for any combination of the deployment parameters. Our numerical analysis reveals that the area spectral efficiency is maximized when the $l \approx 1.4r$. Since $1.4 < \sqrt{3} \approx 1.73$ the network is *fully-connected* due to any transmitting device, regardless its location, being within r of the nearest receiver. Thus, the revealed condition is, in fact, the optimal inter-receiver distance in dense THz networks.

So far we presented results for $f = 1$THz. We now consider a realistic THz channels spanning a certain set of frequencies. Recall that the minimum absorption is observed in the transparency windows described in Section II-A. Fig. 5 shows the average area capacity as a function of r (l is set to the optimal value of $1.4r$) for four transparency windows and the full band 0.1–10THz. Observing the data, we notice that area capacity primarily depends on the channel bandwidth. Thus, the area capacity of the second window, which is the narrowest, is less than the area capacity of 3rd and 4th, even though both absorption and propagation losses are generally lower for the 2nd window, as shown in Fig. 1. We also note that while the area capacity of all considered transparency windows is around 20–100$Tbps/mm^2$, the full band area capacity can theoretically reach the enormous value of two petabits per second per square millimeter, which is absolutely sufficient for any imaginable application suggested for wireless networks.

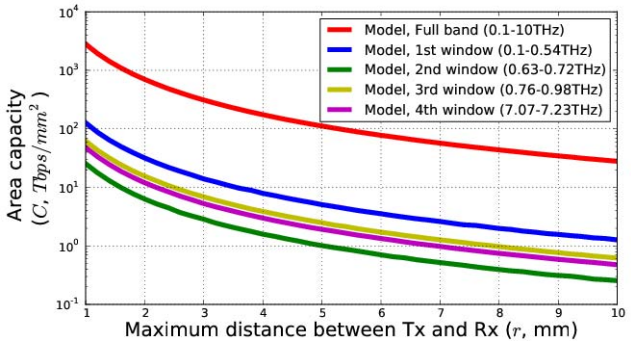

Fig. 5. The area capacity versus maximum distance in the THz network.

VI. Conclusions

In this paper, the interference and spatial channel reuse in ultra-dense randomly deployed THz wireless networks have been studied. We have analyzed the IoNT scenario with multiple simultaneously active links between neighboring devices in terms of SINR and spectral efficiency. To perform this study, we have developed a novel network-level analytical model based on the mathematical apparatus of stochastic geometry.

Our investigations reveal that there is an optimal distance between the receiving devices that maximizes the area capacity and, thus, minimizes the message transmission time. The presented numerical results and conclusions have been independently confirmed by analytical modeling of the considered scenario. The presented evaluation provides an important contribution to the IoNT concept definition and inspires further network-level analysis of THz wireless communications.

Appendix

Below, we introduce the general method of finding functions of random variables that is extensively used in this paper. Let $\boldsymbol{\xi} = (\xi_1, \xi_2, \ldots, \xi_n)$ be the set of random variables with joint pdf $w_{\boldsymbol{\xi}}(\boldsymbol{x})$. Let

$$y_k = f_k(\boldsymbol{x}),\ k = 1, 2, \ldots, n, \tag{38}$$

i.e., we are looking for joint pdf of n random variables as a function of other n variables. Using (38), we can obtain the joint pdf $W_{\boldsymbol{\eta}}(\boldsymbol{y})$ of $\boldsymbol{\eta} = (\eta_1, \eta_2, \ldots, \eta_n)$, where $\eta_k = f_k(\boldsymbol{\xi})$, $k = 1, 2, \ldots, n$. Let now $x_k = \phi_k(\boldsymbol{y}), k = 1, 2, \ldots, n$, be the inverse of (38), that is, $\phi_k = f_k^{-1}$. ϕ_k can be multivalued having a number of branches. Denote the ith branch by

$$x_{k,i} = \phi_{k,i}(\boldsymbol{y}), k = 1, 2, \ldots, n, i = 1, 2, \ldots. \tag{39}$$

Observe that $\boldsymbol{\eta}$ can be considered as a point in n-dimensional Euclidean space. Define B as the event consisting in point $\boldsymbol{\eta}$ falling into n-dimensional subspace S_y. The probability of this even consists of contributions of all the branches of ϕ_k. Defining A_i as $\boldsymbol{\xi} \in S_{x_i},\ i = 1, 2, \ldots,$ we see that $B = \cup_i A_i$ and $A_i \cap A_j = \emptyset,\ i \neq j$, implying that

$$\mathrm{P}\{B\} = V_y = \sum_{\forall i} V_{x_i} = \sum_{\forall i} \mathrm{P}\{A_i\}, \tag{40}$$

where V_y is the n-dimensional volume. Assuming small volumes of S_{x_i} and S_y, V_i can be approximated by

$$V_y \approx W_{\boldsymbol{\eta}}(\boldsymbol{y}) S_y,\ V_{x_i} \approx w_{\boldsymbol{\eta}}(\boldsymbol{x}_i) S_{x_i}. \tag{41}$$

The limit of the ratio S_{x_i}/S_y is expressed via Jacobian

$$J_i = \frac{\partial(x_{1,i}, \ldots, x_{n,i})}{\partial(y_1, \ldots, y_n)}, i = 1, 2, \ldots. \tag{42}$$

Finally, from (40)-(42) we have jpdf as

$$W_{\boldsymbol{\eta}}(\boldsymbol{y}) = \sum_{\forall i} w_{\boldsymbol{\xi}}(\phi_{1,i}(\boldsymbol{y}), \ldots, \phi_{n,i}(\boldsymbol{y})) J_i. \tag{43}$$

When the resulting set of random variables has fewer elements than the initial set, we first introduce auxiliary variables such that both sets have the same number of variables. The solution is then similar to what we outlined above except for the last step, where we integrate over all the auxiliary variables.

Acknowledgment

This work was supported by Academy of Finland FiDiPro program "Nanocommunication Networks", 2012 – 2016.

References

[1] G. P. Fettweis, "The tactile internet: Applications and challenges," *IEEE Vehicular Technology Magazine*, vol. 9, no. 1, pp. 64–70, 2014.

[2] I. Akyildiz and J. Jornet, "The Internet of nano-things," *IEEE Wireless Communications*, vol. 17, no. 6, pp. 58–63, 2010.

[3] J. M. Jornet and I. F. Akyildiz, "Channel modeling and capacity analysis for electromagnetic wireless nanonetworks in the terahertz band," *IEEE Trans. on Wireless Communications*, vol. 10, pp. 3211–3221, 2011.

[4] M. Natrella, O. Mitrofanov, R. Mueckstein, C. Graham, C. C. Renaud, and A. J. Seeds, "Modelling of surface waves on a THz antenna detected by a near-field probe," 2012.

[5] M. Jornet and M. Akyildiz, "Channel modeling and capacity analysis for electromagnetic wireless nanonetworks in the terahertz band," *IEEE Trans. Wir. Comm.*, vol. 10, pp. 3211–3221, Oct. 2011.

[6] J. Jornet and I. Akyldiz, "Femtosecond-long pulse-based modulation for terahertz band communication in nanonetworks," *IEEE Trans. Comm.*, vol. 62, pp. 1742–1754, May 2014.

[7] www.cfa.harvard.edu, "Hitran: High-resolution transmission molecular absorption database," tech. rep., Harvard-Smith. Astroph. Center, 2014.

[8] L. Kish, "Stealth communication: Zero-power classical communication, zero-quantum quantum communication and environmental-noise communication," *Appl. Phys. Let.*, vol. 87, 2005.

[9] P. Boronin, V. Petrov, D. Moltchanov, Y. Koucheryavy, and J. Jornet, "Capacity and throughput analysis of nanoscale machine communication through transparency windows in the terahertz band," *Elsevier Nano Communication Networks*, vol. 5, pp. 72–82, Sept. 2014.

[10] X. Wang and T. Berger, "Spatial channel reuse in wireless sensor networks," *Teor. Ver. Prim.*, vol. 14, no. 2, pp. 133–146, 2006.

[11] X. Guo, S. Roy, and W. Conner, "Spatial reuse in wireless ad-hoc networks," in *In Proc. VTC-Fall*, pp. 1437–1442, 2003.

[12] X. Lin, J. Andrews, and A. Ghosh, "Spectrum sharing for device-to-device communication in cellular networks," *IEEE Trans. Wir. Comm.*, vol. 13, no. 12, pp. 6727–6740, 2014.

[13] J. Andrews, K. Ganti, M. Haenggi, N. Jindal, and S. Weber, "A primer on spatial modeling and analysis in wireless networks," *IEEE Comm. Mag.*, vol. 48, pp. 156–163, Nov. 2010.

[14] M. Haenggi, J. Andrews, F. Baccelli, O. Dousse, and M. Franceschetti, "Stochastic geometry and random graphs for the analysis and design of wireless networks," *IEEE JSAC*, vol. 27, pp. 1029–1046, Nov. 2009.

[15] A.-M. Mathai, *An introduction to geometrical probability: distributional aspects with applications*, vol. 1. CRC Press, 3rd ed., 1999.

[16] W. Feller, *An introduction to probability theory and its applications*, vol. 1. Wiley, 3rd ed., 1968.

[17] M. Abramowitz and I. Stegun, *Handbook of Mathematical Functions with Formulas, Graphs, and Mathematical Tables*. Dover, 1965.